MURA 542-75

Reprinted from
Proceedings of the Intern. Conf.
High-Energy Accelerators and
Instrumentation - CERN 1959

Fermilab Library
0 1160 0038828 4

# EXPERIENCE WITH A SPIRAL SECTOR FFAG ELECTRON ACCELERATOR

**R. O. Haxby** (*), **L. J. Laslett** (**), **F. E. Mills, F. L. Peterson, E. M. Rowe and W. A. Wallenmeyer**

Midwestern Universities Research Association, Madison, Wis. (***)

*(presented by K. R. Symon)*

## I. INTRODUCTION

In fixed-field alternating gradient (FFAG) accelerators [1-4], particles with a large range of momenta can be accommodated simultaneously within an annular magnet of limited radial extent, thus providing a desirable flexibility in the methods of accelerating the particles and affording the promise of high beam intensities. The spiral sector type is an attractive form of FFAG accelerator, since a smaller circumference factor may be employed than is feasible with the radial sector design and a significant economy thus can be obtained in the construction. A six-sector spiral ridge FFAG accelerator has been constructed and successfully operated to accelerate electrons from 35 to 180 keV kinetic energy [5, 6]. Acceleration was by betatron action, supplemented by radio-frequency acceleration when desired. The design was based on magnetostatic and orbit computations (****), and the subsequent performance was found to be in good accord with these computations. The model permitted not only the acquisition of design experience and the demonstration of predicted stability regions, but also afforded the opportunity of studying coupling and multi-particle effects not investigated in detail theoretically.

The number of sectors ($N$) was selected as 6, in the interests of a conservative design, and the remaining basic parameters characterizing the model then were selected on the basis of digital computations pertaining to the magnetostatic problem and to the orbit dynamics in the resultant magnetic field. The inner radius of the accelerator was determined by the need to accommodate the betatron core and for convenience of access to ancillary components, while the strength of the magnetic field at that radius was dictated by the selection of 35 keV as a convenient injection energy. The maximum energy attainable by the model ($\simeq$ 180 keV) was sufficiently greater than the transition energy (155 keV) so that experience was obtained in the use of radio-frequency programs suitable for traversing this possibly critical region.

## II. DESIGN

A separated-sector magnet design was adopted in the interests of simplicity and to achieve conveniently a field with a large azimuthal variation such as would be expected to affect favorably the non-linear stability limits [4]. Guard rings, effectively at zero magnetostatic potential, further enhanced the field variation and, secondarily, provided some additional shielding from external magnetic fields present in the laboratory. The character of the magnetic field which would result from specific magnet structures of this type (Fig. 1) was determined computationally by a relaxation

(*) On leave of absence from Purdue University, Lafayette, Indiana.

(**) Iowa State University, Ames, Iowa.

(***) Supported by the United States Atomic Energy Commission.

(****) The computations were primarily made by aid of the electronic digital computer of the Graduate College of the University of Illinois (ILLIAC), corroborated and supplemented by later computations made with the IBM-704 computer in the MURA Laboratory at Madison. The invaluable contributions to this work by J. N. Snyder and A. M. Sessler are gratefully acknowledged, as is also the cooperation of J. P. Nash, R. E. Meagher, and others at the University of Illinois, who facilitated initiation of this work.

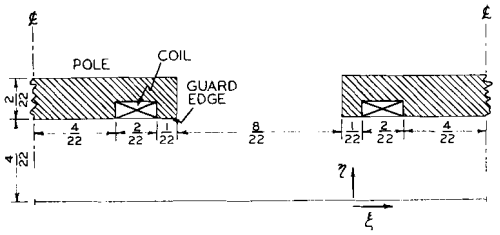


**Fig. 1** Cross section of magnet pole. $\xi = \frac{1}{2\pi}\left[\frac{1}{w}\ln\frac{r}{r_o} - N\theta\right]$ and $\eta = \frac{[(1/w)^2 + N^2]^{1/2}}{2\pi}\frac{z}{r}$. Where $r$, $\theta$, $z$ are cylindrical coordinates, and $w$ is the spatial period radially divided by $2\pi r$. The pole profile in the $\xi$, $\eta$ -plane represents a section taken at constant radius, but with *unequal scale factors* in the azimuthal and axial directions. The outline represents more truly a cross section *perpendicular* to the spiral save that the general increase of all linear dimensions with radius is not depicted. Azimuthal distances at constant radius are given by $2\pi r/N$ times the increment of $\xi$ and axial distances by $2\pi r[(1/w)^2 + N^2]^{1/2}$ times the increment of $\eta$. For the present model $1/w = 6.25$ and these distances become $1.0472\, r\Delta\xi$ and $0.7252\, r\Delta\eta$, respectively.

procedure, wherein it was possible to employ a two-dimensional mesh [7] by taking advantage of the scaling feature of the field. The resultant magnetostatic potential, suitably scaled, was then stored in the computer memory for use in orbit computations.

Three operating points considered in the design of the model are indicated on Fig. 2, where the abscissa and ordinate $(\sigma_x, \sigma_y)$ of each point respectively denote the phase change per sector of the radial and axial betatron oscillations. Studies of orbit dynamics for point A of Fig. 2 indicated strong coupling of radial to axial motion, a behaviour attributed to the proximity to the $\sigma_x = 2\sigma_y$ resonance. The coupling was found to be less pronounced for point B, but the radial stability limit was found to be rather small ($\simeq r/25$) and the value of $\sigma_y$ was also undesirably low. The operation point chosen

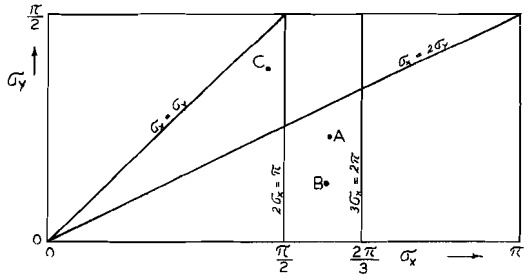


**Fig. 2** Location of operating points for which detailed computations were made. For these three points the phase changes per sector of the betatron oscillations, $\sigma$, were as follows: A (0.597 $\pi$, 0.225 $\pi$), B (0.595 $\pi$, 0.129 $\pi$), C (0.466 $\pi$, 0.375 $\pi$).

for the model was, accordingly, that denoted by point C on Fig. 2 ($\sigma_x = 0.466\pi$, $\sigma_y = 0.375\pi$), situated a considerable distance *above* the $\sigma_x = 2\sigma_y$ resonance. Here the stability region was found to be at least as large as for point A and the axial oscillation frequency was more acceptable; coupling effects, moreover, were no longer apparent and the sensitivity to misalignments (such as sector displacements) appeared to be much less pronounced. In practice, the model was provided with tuning coils to permit an experimental investigation of performance for operation under other conditions, in order that the effect of various resonance lines in the neighbourhood of point C could be determined.

TABLE I

Parameters of the spiral sector model

| *Parameter* | *Symbol* | *Value* |
|---|---|---|
| Number of sectors | $N$ | 6 |
| Mean field index | $k$ | |
| $k = (r/\langle B\rangle_{av})(\partial\langle B\rangle_{av}/\partial r)$ | | |
| design value | | 0.7 |
| adjustable within the range | | 0.2 to 1.16 |
| Spatial period, radially/$2\pi r$ | $w$ | 0.16 |
| Spiral angle with radius | $\zeta$ | 46° |
| $\cot\zeta = Nw$ | | |
| Field flutter | $f_{eff}$ | |
| $f_{eff} = [2\langle(B - \langle B\rangle_{av})^2\rangle_{av}/\langle B\rangle^2_{av}]^{1/2}$ | | |
| design value | | 1.087 |
| adjustable within the range | | 0.57 to 1.60 |
| Betatron oscillations per revolution | | |
| $\nu = N\sigma/2\pi$ | | |
| radial, design value | $\nu_x$ | 1.398 |
| axial, design value | $\nu_y$ | 1.125 |
| Vacuum chamber dimensions, interior : | | |
| inner radius | $r_1$ | 27 cm |
| outer radius | $r_2$ | 55 cm |
| height | $h$ | 3.8 cm |
| Injection radius | $ri$ | 31 cm |
| Detector radius, useful, maximum | $rf$ | 52 cm |
| Injection energy, nominal | $Ei$ | 35 keV |
| Final Energy | $E_f$ | |
| at $k = 0.7$ | | 124 keV |
| at $k = 1.16$ | | 180 keV |
| Transition energy | $E_t$ | 155 keV |
| Revolution frequency, maximum | $f_t$ | 62.45 Mc/s |
| Radial stability limit/$r$, computed | $Ax$ | $\pm$ 0.11 |
| (near the center of a radially-focusing region and when the radial momentum has the value corresponding to the stable fixed point. The radial motion at the limit of stability actually covers a range $\Delta r/r = \pm$ 0.18 at this azimuth.) | | |

The basic parameters of the model are given in Table I and a general view of the assembled accelerator is shown in Fig. 3. The brass vacuum chamber was constructed as two hollow semi-circular annuli, insulated from each other, so that the accelerating

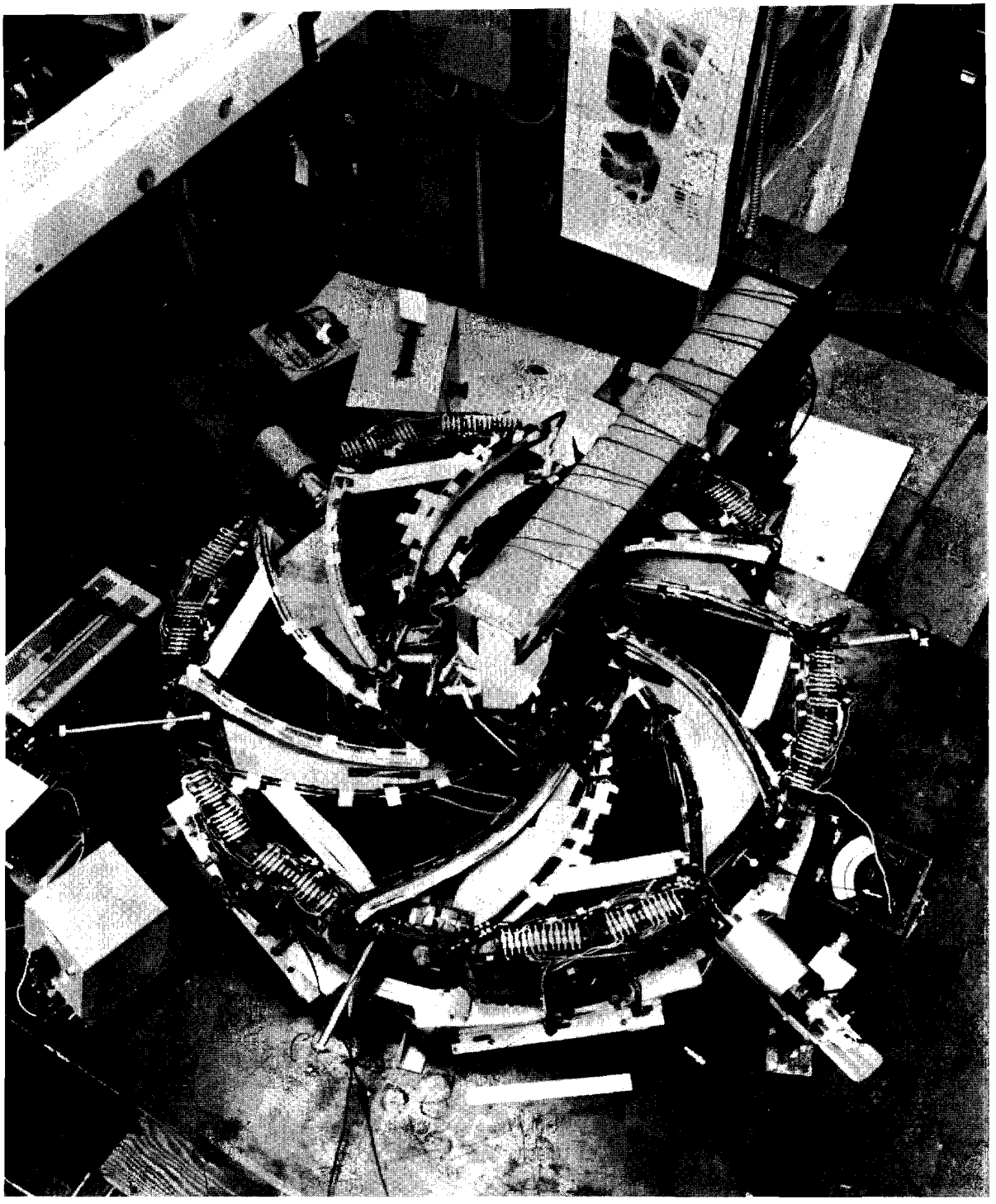

**Fig. 3** View of the assembled spiral sector accelerator.

voltages could be applied. A movable scintillation detector and a current probe were provided for detection and analysis of the accelerated beam. An additional probe carried an offset molybdenum wire which, by rotation about the probe axis, served to measure the vertical location of the equilibrium orbit, to indicate the amplitude of the axial oscillations, and to limit these amplitudes when desired. Various electrodes were also provided to permit the application of auxiliary perturbing fields required for some of the performance tests.

## III. PERFORMANCE

### A. Intensity survey

Following assembly of the model, and after careful measurement and correction of the magnetic field, a betatron-accelerated beam was immediately obtained. Tests were then made to determine the betatron oscillation frequencies and the variation of beam intensity over the accessible portion of the $\nu_x$, $\nu_y$ stability region. The oscillation frequencies were determined in this work by the method[8,9] of resonant radio-frequency enhancement of the betatron oscillations. The value of $\nu_y$ was found to vary significantly with amplitude (axial or radial amplitude) and an estimated 1 to 2 per cent inaccuracy arose from this effect in the intensity survey. The betatron oscillation frequencies observed in the model, without current in the tuning coils, were close to the values resulting from the digital computations (*see above*) and a small current in the flutter-tuning coils sufficient to raise $f_{\text{eff}}$ from 1.03 to its design value of 1.087 raised $\nu_y$ from 1.026 to the predicted value of 1.12. The resonance diagram which resulted from the intensity survey, with low emission from the injector, is shown in Fig. 4. A sizable region of maximum intensity is seen to occur centered about the design point and the importance of several resonances which cross the accessible region is also apparent.

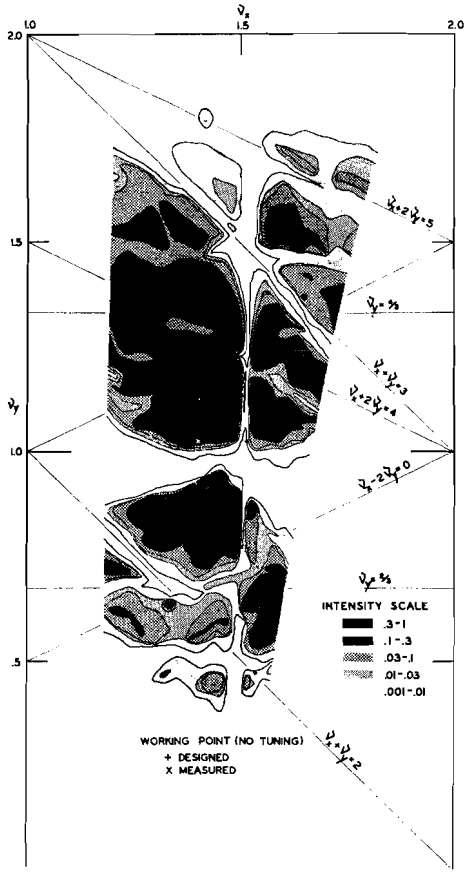


**Fig. 4** Beam intensity as determined by the resonance survey of the spiral sector model, using low emission from the injector. + denotes the design values for the oscillation frequencies and is seen to be surrounded by a sizable region of high intensity. The strong influence of several resonances is also evident, the occasional slight departure of the resonance lines from the positions of minimum intensity being believed chiefly ascribable to the imprecise scaling of the field when substantial tuning currents are applied.

### B. Stability limits

In measuring the radial stability limits in a fixed-field accelerator, one may examine the range of energies throughout which particles can be captured at the injection radius. On the supposition that the minimum-energy particles are injected into an equilibrium orbit which just misses the injector and that the maximum-energy particles oscillate about an equilibrium orbit which is situated a distance away from the injector equal to the stability limit, a measurement of this energy difference—or, equivalently, of the variation in the time taken for acceleration—permits the stability limit to be calculated.

The calculation to convert the variation of the required acceleration time to the radial range of stable motion at the injection radius requires use of the known rate of acceleration (betatron voltage) and correction for the adiabatic damping which occurs in the course of acceleration ($\propto B^{-1/2}$). With either method it must be recognized that the spatial stability limits will vary with azimuth, due to the alternating-gradient nature of the magnetic focusing.

The axial stability limits may be measured directly by use of the vertical-scanning probe mentioned previously (Sect. II).

1) Results at the design point

A measurement of the radial stability limit by the second of the methods described led to a value at the azimuth of the injector (near the center of a radially-defocusing region) given by $\pm 0.058\,r$, or $\pm 1.75$ cm, for the design point. This limit corresponds approximately to $\pm 0.08\,r$ at the azimuth to which the entry in Table I pertains and is in reasonable agreement with the computational value reported there for operation in the absence of all imperfections. The measured value for the axial stability limit at the injector similarly was $\pm 0.045\,r$ This result is somewhat smaller than the maximum amplitude which would be permitted by the internal dimension of the vacuum chamber ($\pm 0.061\,r$). as would necessarily be expected if the magnetic median plane were not quite centrally located within the vacuum chamber, while the computational study suggested a dynamical limit at the injector somewhat greater than the available aperture.

2) Performance near the $\sigma_x = 2\sigma_y$ resonance

Although, as indicated previously, (Sect. II), the design of the model was deliberately chosen to avoid the $\sigma_x = 2\sigma_y$ resonance, there is an obvious interest in experimental information concerning effects attributable to this difference resonance in spiral sector synchrotrons [10-12] to complement the analytic studies of Walkinshaw [13] and others [14, 21]. Unfortunately for this purpose, the accessible portion of the resonance line was of rather limited extent (shown on Fig. 4) and fell in a region where other important resonances were also present. Observations of some interest were made, however, near the $\sigma_x = 2\sigma_y$ resonance with $\nu_x \simeq 1.46$ and the results were interpreted in the light of computational results obtained specifically for $\nu_x = 1.25$, $\nu_y = 0.62$.

From the computations it appeared that the radial motion, if present alone, would have very generous stability limits, but, as is typical of performance on a coupling resonance [10-12], a very small amount of radial oscillation would be accompanied by a marked (exponential) growth of axial oscillations to quite large values. In the example studied it was found that a radial amplitude in excess of about $0.022\,r$, or about 0.7 cm measured at the injector, would engender axial displacements in excess of $0.06\,r$ (1.9 cm) and so result in interception of the beam by the chamber wall. If the wall were not present, this physical limitation of course would not occur and stable motion with axial amplitudes up to about $0.1\,r$ might then be considered possible.

Experimental measurement at the operating point considered in the computations led to an effective radial stability limit of 0.5 cm and, as was the case for the design point, axial amplitudes in excess of 1.3 cm were found. In more detailed measurements, made with $\nu_x \simeq 1.46$, the radial stability indeed appeared definitely to decrease if the axial excursions were limited by the vertical-scanning probe, the effect being more pronounced when operating very close to the resonance line (Fig. 5). The foregoing results thus appear to substantiate the view that, in practice, the growth of axial amplitude associated with operation near the $\sigma_x = 2\sigma_y$ difference resonance can markedly curtail the region of stability and thereby effect a pronounced loss of intensity.

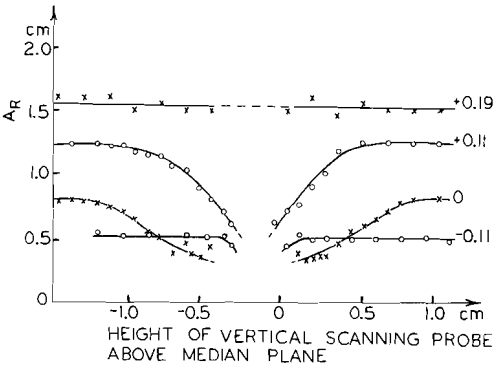


**Fig. 5** Observed apparent radial stability limits ($A_R$) as affected by restricted axial motion, for operation near the $\nu_x = 2\nu_y$ resonance with $\nu_x \simeq 1.46$. The number appended to an individual curve denotes the value of $2\nu_y - \nu_x$.

3) Effect of misalignments

To complement a portion of the computational studies concerning the spiral sector model, the effects of certain deliberately introduced imperfections were investigated experimentally at the design point. By decreasing the field strength in one entire sector by 7 per cent, the radial and axial stability limits appeared to become reduced by approximately 20 or 25 per cent, and a similar effect on the radial

limit was seen when one sector was displaced axially by 1 mm. It has recently appeared possible by analytic means [15] to account reasonably well for some of the results obtained in these perturbation studies.

### C. Injection methods

The injector assembly provided for the spiral sector model employed an electron gun unit which directed a focused electron beam into a deflector system. The deflection system, which provided a 15-degree deflection, permitted injection of a beam 2 mm wide $\times$ 9 mm high from a region directly behind a grounded septum 0.1 mm thick. Although the axial admittances [16, 17] of the injector and the accelerator were reasonably well matched, the radial admittance of the accelerator was some 90 times that of the injector (18 mm $\times$ rad vs. 0.2 mm $\times$ rad) and it accordingly was reasonable to consider multi-turn injection [see paragraph (b) below].

#### 1) Short-pulse injection

(a) One method employed for injection undertook to accelerate the electrons rapidly, but under conditions such that the amplitudes of the radial betatron oscillations remained smaller than the radial width of the beam due to energy spread. With an acceleration voltage of 150 V/turn, successful injection of more than $10^{10}$ electrons was accomplished in a 4 $\mu$s interval and the corresponding electron density estimated as $3\times10^{6}$ cm$^{-3}$. It is noteworthy that at operating points such that one of the oscillation frequencies lies *below* a resonance by an amount sufficiently small to preclude obtaining a beam at low emission currents, use of higher emission has been seen to permit a beam to be established. The observation of phenomena such as this in the electron model suggests that, with high emission currents from the injector, limitations due to space-charge forces can be encountered.

If one estimates the change of oscillation frequency due to space-charge forces in the geometrically-simple case of a flat beam of uniform density [18], neglecting alternating-gradient effects in the calculation, one obtains as the limiting particle density

$$n = \frac{1}{4\pi r_0 R_0^2}\beta^2\nu^3\left|\delta(\nu_z^2)\right|, \quad (\beta = v/c\,, \quad \gamma = E/mc^2) \qquad (1)$$

where $r_0$ denotes the "classical radius" of the particle, $R_0$ is the radius of the orbit, and $\delta(\nu_z^2)$ denotes the permissible decrease of the square of the oscillation frequency. For comparison with the work reported in the preceding paragraph, we note that $\delta(\nu_y^2) = -0.2656$ would carry the operating point to the $\nu_y = 1$ resonance and a change of about $-0.2$ might be considered sufficient to reach the stop band associated with this integral resonance (Fig. 4). For the injection conditions pertaining to the model, then, Eq. (1) suggests a space-charge limit of approximately $9\times10^{6}$ cm$^{-3}$, or about three times that inferred from the experiment reported above.

(b) A second successful injection method did not require acceleration of the electrons, but employed an azimuthally localized, time dependent radial electric field to perturb the equilibrium orbit. Under suitable conditions the beam could then be moved away from the injector adiabatically, by decreasing the strength of the perturbation, and beam densities of approximately one-sixth the estimated space-charge limit (Eq. (1)) were realized.

#### 2) Long-pulse injection

Because of the attractive possibility of achieving high intensities by protracted injection into FFAG betatrons [1-3], and because of the inherent interest in space-charge problems, arrangements were made to permit the injection of high intensity beams into the electron model for time intervals typically 400 $\mu$s long at the peak of the accelerating voltage wave.

At the start of the injection process the beam current is found virtually immediately to attain a value, $I_0$, which is presumably limited by inter-electron space-charge forces and is controlled by the nearest *lower-lying* resonance, as discussed above. Subsequently, as ions are formed in the residual chamber gas and begin to neutralize the mutual electrostatic interactions of the electrons, a higher current, $I_{max}$, can be reached and its value may be considered as determined by the limited emission from the injector. At still later times sufficient neutralization can have occurred to move one of the oscillation frequencies into the stopband associated with the nearest *higher-lying* resonance and the beam will then promptly be lost regeneratively (Fig. 6). In substantiation of this suggested sequence of events it was observed (i) that the rate of rise of current from $I_0$ to $I_{max}$, and the value of $I_{max}$ itself, each increase with the emission current and

**Fig. 6** Typical oscillogram of beam current, measured at the target under conditions of high emission such that periodic instability develops from charge neutralization.

(ii) the time interval before the beam disappears is inversely proportional to the product of pressure and emission. More directly, moreover, with high emission it is observed by radio-frequency measurements of the betatron oscillation frequencies that these frequencies indeed do decrease at first and later rise, to values above those prevailing at low emission, typically approaching a half-integral value (*e.g.*, $\nu_x = 1.5$) at the time the beam is destroyed.

Following loss of the beam in the manner just described, a definite time interval must elapse — during which a fraction of the positive ions presumably migrate to the chamber walls — following which the current $I_{max}$ is suddenly established again. As before, this current $I_{max}$ lasts only for a time before being destroyed and this process has been observed to continue in a reproducible periodic fashion as long as the emission and accelerating voltage are both present.

Despite the interpretability of the aforementioned phenomena when the relevant parameters are carefully controlled, it must be reported, however, that additional complex phenomena involving the collective motion of particles evidently occur. Thus, for example, a strong radio-frequency field was found to arise from the beam. The frequencies of this radiation were usually half-integral multiples of the electron revolution frequency at the injection radius, but the detailed characteristics depended markedly on the operating point of the accelerator and the intensity was particularly strong at the time when the beam became destroyed. It is, moreover, of some interest to note that, in one observation, it appeared that the current which arrived at the target was bunched at the revolution frequency of the electrons.

D. Studies of radio-frequency acceleration

In previous work[19] with an electron model of a *radial* sector FFAG accelerator[9], experience had been obtained with particle-handling techniques (as beam stacking[1, 2, 20]) in a FFAG accelerator. The objective of the radio-frequency acceleration experiments, which we describe below, was specifically to determine the frequency-modulation programs which could be applied most successfully to accelerate electrons through the transition energy. To implement this investigation it was convenient to excite the betatron core from a double-pulse power supply, so that electrons could thereby be accelerated in two stages and radio-frequency fields applied in the interim.

The effectiveness of various frequency-modulation programs was determined by the method used earlier in similar studies[19] with a radial sector model[9]. Electrons are carried to an energy of about 118 keV — i.e., below the transition energy — by the first betatron pulse and then subjected to the radio-frequency field prior to the onset of the second betatron pulse. That fraction of the electrons which in this way is successfully carried through the transition energy will then arrive at the target before the second betatron pulse is applied, while those electrons not carried beyond the transition energy are brought to the target somewhat later by this second pulse and those not captured by the radio-frequency at all appear at a still later time (Fig. 7). A frequency program which overshot the transition frequency in an appropriately controlled way was successful

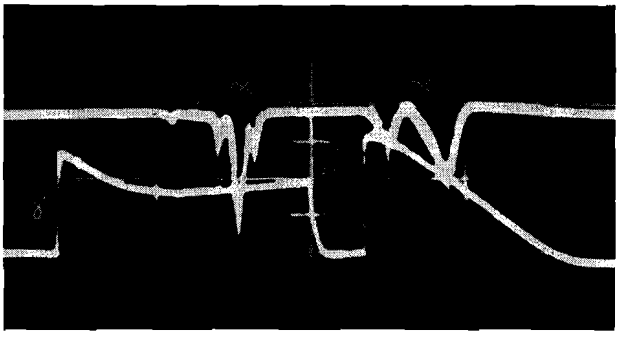

**Fig. 7** Oscillographic records of ($\alpha$) the beam received at the detector, ($\beta$) the betatron voltage, and ($\gamma$) the envelope of the radio-frequency voltage in experiments designed to investigate acceleration through the transition energy. The beam trace indicates that a fraction of the electrons have been accelerated successfully through the transition energy, to arrive at the detector prior to the onset of the betatron pulse ($\beta$).

in carrying about 60 per cent of the accelerated electrons through the transition energy and on to the target.

## IV. CONCLUSION

The experience gained in the construction and experimental work with the spiral sector model not only has served to enhance our appreciation of detailed problems associated with the design of FFAG accelerators and to demonstrate the predictable characteristics of a spiral sector machine, but has also afforded valuable information concerning which definitive results were not obtainable by analytic or computational methods. The successful outcome of the model program has resulted from the contributions of many individuals who have devoted their efforts to the MURA group at various times during the past three years. It is impossible to acknowledge these contributions individually here, but, in addition to those of whom we have already made mention in this paper, we would especially like to thank Dr. F. T. Cole, of the State University of Iowa; Mr. E. A. Day, of the General Atomic Division, General Dynamics Corporation; Drs. H. J. Hausman and C. E. Nielsen, of the Ohio State University; Dr. T. Ohkawa, of the University of Tokyo; Mr. D. S. Roiseland, of the University of Wisconsin; Dr. R. Stump, of the University of Kansas; and, most particularly, both Dr. D. W. Kerst, of General Atomic, for his invaluable direction of the entire design and constructional phases of the program, and Dr. K. R. Symon, the Technical Director of the MURA group, for his continued interest and help in this work from its inception.

## LIST OF REFERENCES


1. Symon, K. R., Kerst, D. W., Jones, L. W., Laslett, L. J. and Terwilliger, K. M. Fixed-field alternating-gradient particle accelerators. Phys. Rev., *103*, p. 1837-59, 1956.
2. Laslett, L. J. Fixed-field alternating-gradient accelerators. Science, *124*, p. 781-7, 1956.
3. Kerst, D. W., Symon, K. R., Laslett, L. J., Jones, L. W. and Terwilliger, K. M. Fixed field alternating gradient particle accelerators. CERN Symp. 1956. *1*, p. 32-5.
4. Kerst, D. W. Spiral sector magnets. CERN Symp. 1956. *1*, p. 366-75.
5. Kerst, D. W., Hausman, H. J., Haxby, R. O., Laslett, L. J., Mills, F. E., Ohkawa, T., Peterson, F. L., Sessler, A. M., Snyder, J. N. and Wallenmeyer, W. A. Operation of a spiral sector fixed field alternating gradient accelerator. Rev. sci. Instrum., *28*, p. 970-1, 1957.
6. Kerst, D. W. et al. Electron model of a spiral sector accelerator. (to be published).
7. Laslett, L. J. and Symon, K. R. Particle orbits in fixed field alternating gradient accelerators. CERN Symp. 1956. *1*, p. 286.
8. Hammer, C. L., Pidd, R. W. and Terwilliger, K. M. Betatron oscillations in the synchrotron. Rev. sci. Instrum., *26*, p. 555-6, 1955.
9. Cole, F. T., Haxby, R. O., Jones, L. W., Pruett, C. H. and Terwilliger, K. M. Electron model fixed field alternating gradient accelerator. Rev. sci. Instrum., *28*, p. 403-20, 1957.
10. Laslett, L. J. and Symon, K. R. Particle orbits in fixed field alternating gradient accelerators. CERN Symp. 1956. *1*, p. 287-9.
11. Laslett, L. J. and Sessler, A. M. Concerning coupling resonances in the spirally-ridged FFAG accelerator. MURA (*) 263. May 6, 1957.
12. Laslett, L. J. Computational examples of solutions to differential equations which simulate growth of axial oscillations in an FFAG accelerator operated near the $\sigma_x = 2\sigma_y$ resonance. MURA (*) 295. June 7, 1957.
13. Walkinshaw, W. A spiral ridged Bevatron. AERE, Harwell, 1955. (unpublished).
14. Hagedorn, R. Note on an instability on a difference resonance line. CERN Symp. 1956. *1*, p. 293-4.
15. Kerst, D. W. et al. Electron model of a spiral sector accelerator. See Parzen, G. Appendix III. (to be published).
16. Sigurgeirsson, T. Betatron oscillations in the strong focussing synchrotron. CERN / T (**) / TS2. December, 1952. p. 9-10.
17. Courant, E. D. and Snyder, H. S. Theory of the alternating-gradient synchrotron. Ann. Phys. New York, *3*, p. 12, 1958. (Equation (3.23))
18. Laslett, L. J. Discussion of space-charge effects in the alternate-gradient synchrotron. MURA (*) 14. January 1954. Equations (4) and (5). (This report considers a *toroidal* beam of uniform density for which the attainable charge density is double that for the flat beam with which we are concerned in the present paper.)
19. Terwilliger, K. M., Jones, L. W. and Pruett, C. H. Beam stacking experiments in an electron model FFAG accelerator. Rev. sci. Instrum., *28*, p. 987-97, 1957.
20. Symon, K. R. and Sessler, A. M. Methods of radio frequency acceleration in fixed field accelerators with applications to high current and intersecting beam accelerators. CERN Symp. 1956. *1*, p. 44-58.
21. Meier, H. and Symon, K. R. Analytical and computational studies on interaction of a sum and difference resonance. See p. 253.


(*) See note on reports, p. 696.

(**) Internal memoranda not generally distributed but possibly available from author.